national accelerator laboratory

NAL-Pub-73/78-EXP
2050.000

(Submitted to Phys. Rev. Letters)

THE ENERGY DEPENDENCE OF BACKWARD $\pi^+ p$ ELASTIC SCATTERING FROM 2 TO 6 GeV/c

W. F. Baker, D. P. Eartly, K. P. Pretzl,
S. M. Pruss, and A. A. Wehmann
National Accelerator Laboratory, Batavia, Illinois 60510

P. Koehler
Argonne National Laboratory, Argonne, Illinois 60439

and

A. J. Lennox, J. A. Poirier, C. A. Rey, and O. R. Sander
University of Notre Dame, Notre Dame, Indiana 46556

December 1973

ABSTRACT

The energy dependence of backward π^+p elastic scattering has been measured for incident pion momenta from 2.0 to 6.0 GeV/c in steps of typically 100 MeV/c. Values are presented for both the differential cross section extrapolated to 180^o and the slope of the backward peak as a function of momentum. In the s channel we see the effects of the established Δ^{++} resonances and evidence for the $\Delta(3230)$. In addition the data show the existence of a negative parity Δ resonance with mass approximately 2200 MeV/c^2.

Numerous experiments have measured the angular distributions of backward elastically scattered pions at various energies. Systematic studies[1-3] of the energy dependence of the backward elastic scattering of negative pions have been made up to 5.3 GeV/c. Similar studies[3-7] for positive pions have the added difficulty of separating the recoil protons from a positive beam. In this experiment, a focusing spectrometer separated the forward going recoil protons from beam momentum particles. Scintillation counter hodoscopes could then be used, permitting the high beam intensities required for an adequate event rate.

A layout of the apparatus at the Zero Gradient Synchrotron of the Argonne National Laboratory is given in Figure 1. The incident pions were identified by scintillation counters and two threshold Cerenkov counters. Positrons in the beam were vetoed by an additional Cerenkov counter further upstream. The scatterings took place in a liquid hydrogen target 2" in diameter and 10" long, and were measured in the vertical plane. The backward scattered pions were located in both azimuthal, ϕ^B, and polar, θ^B, angles by a scintillation counter hodoscope below the incident beam line. This hodoscope separated the pions into six angular bins of θ^B from about 141^o to 173^o. Similarly the forward going recoil

protons were located by a hodoscope, θ^F, ϕ^F, attached to the entrance face of the first quadrupole magnet of the spectrometer.

The focusing spectrometer separated the recoil protons from the beam particles and from forward scattered particles. It consisted of two quadrupole magnets separated by a dipole magnet. The first quadrupole was set for vertical focusing and the second for horizontal focusing. This resulted in a horizontal angular acceptance of ± 12 mr and a vertical angular acceptance of ± 45 mr, which yields a solid angle acceptance of 2.2 msr. The axis of the spectrometer was raised above the beam line so that recoil protons could be measured at angles up to 5^o from the beam. The quadrupole magnets imaged the hydrogen target onto the momentum hodoscope, P-HOD. The linear magnification was 5.7 in the vertical plane and 0.17 in the horizontal plane. The dipole magnet deflected the particles horizontally to produce, at the momentum hodoscope, a dispersion of 0.28 cm per percent $\Delta p/p$. This, combined with the horizontal image size and hodoscope counter size, yielded a momentum resolution of $\Delta p/p$ = 2.5% at 3.0 GeV/c, and a spatial separation of 3.0 cm between the recoil protons and the forward scattered or beam particles.

The recoil proton momentum hodoscope contained ten vertical scintillation counters of 6.3 mm width. Beyond

this a threshold Cerenkov counter, C3, counted pions and was put in anticoincidence for backward scattering.

The hydrogen target was placed at the center of a vertically deflecting dipole C magnet. During data taking this magnet was off, but when energized it was used to sweep the beam vertically to measure the transmissivity of the spectrometer as a function of angle.

The length of the spectrometer could be changed by sliding the target assembly, with counters and magnet, on rails provided. Such a move was made only once during the experiment. The initial position was used for incident momenta from 2.0 to 4.6 GeV/c. The spectrometer was then lengthened to extend the measurements to 6.0 GeV/c. At this setting several points were measured at lower energies to check the consistency of the two geometries. The momentum spread, ΔP_o, of the incident beam was typically ± 3/4% and in all cases was less than the momentum separation of the points.

As only counters were used, it was possible to run at beam intensities as high as 3×10^6 particles per ZGS pulse. Approximately one day was spent accumulating data at each beam momentum (1,000 to 13,000 events). Forward scattering was measured concurrently, and served as a continuous, high-rate monitor of the spectrometer system.

Conventional logic circuitry identified events as to angle, coplanarity and momentum, and these rates were recorded on scalers. Latches for the individual counters and their logic combinations were set by an event signal. These were then read into an on-line computer where checks on the data were made and where the data were subsequently recorded on magnetic tape.

Background events resulted from accidental coincidences, inelastic processes and interactions in other materials than liquid hydrogen. Accidentals were continuously monitored with out-of-time coincidence circuits. Most inelastic events were rejected by the momentum hodoscope of the spectrometer since their recoil proton momenta were below that for elastic scattering. Periodic target empty runs determined the number of non-hydrogen interactions. The fraction of events due to all other background processes varied with energy, but typically amounted to 3% of the total.

The geometrical acceptance of the combined pion and proton hodoscopes was calculated with a Monte-Carlo program taking into account the incident beam divergence and other geometrical factors.

The transmissivity used to obtain cross sections was evaluated by a second Monte-Carlo calculation and ranged

between 95 and 100%. The magnet surrounding the target was used to sweep the beam vertically over the spectrometer aperture. This measurement served as a check on the latter Monte-Carlo program. To measure the energy dependence of π^+p backward scattering only the magnet currents were changed. Therefore, any systematic errors should have a minimal energy dependence and are estimated to be ± 5%.

The differential cross sections were calculated from the measurements at each energy for each of the angular bins mentioned above. As these bins were at fixed laboratory angle, their u values varied with energy, but in general the range covered corresponded to the region of positive u. Backward π^+p scattering is characterized by a steep peak dropping from a maximum at 180^o to a minimum at $u = -0.15$ GeV^2. We therefore assumed a simple exponential for the u dependence of our data, $a \cdot e^{bu}$, and extrapolated to 180^o to obtain the differential cross sections plotted in Figure 2. The energy dependence of the slope parameter, b, is given in Figure 3. In this energy range the slope appears to be increasing slowly with beam momentum except for the structure evident between 2.0 and 2.7 GeV/c.

Within the concept of semi-local duality the structure observed in the energy dependence of the π^+p differential

cross section at 180° seems to be best interpreted by s channel resonances with isospin 3/2. The most prominent feature is the $\Delta(2420)$ with the $\Delta(2850)$ appearing as a broad shoulder on its high energy side. The data were fit with a model, similar to that of Ma and Shaw[8], consisting of Breit-Wigner resonance amplitudes superimposed on a non-signatured Regge background term. The parameters of the I = 3/2 Δ resonances used in this fit were taken from reference 9. Interpreting the shoulder centered at approximately 5.1 GeV/c as the $\Delta(3230)$[10], we adjusted its parameters to give a good fit to our data. We thus confirm the existence of the $\Delta(3230)$ which SU(6) predicts to have spin 19/2.

On the low side of the $\Delta(2420)$ peak the cross section drops to a deep minimum at P_o = 2.1 GeV/c and then rises toward the $\Delta(1950)$. Attempts to fit the data with positive parity Δ_δ resonances alone were unsuccessful in this region, the resultant dip being an order of magnitude too shallow. The data could only be fit by introducing a negative parity Δ resonance with a mass of approximately 2200 MeV/c^2.

We wish to thank our former collaborator, Dr. George Burleson, for his participation in the preparatory phases of this experiment and Dr. David Carey for the use of his program, TURTLE. It is a pleasure to thank Dr. Bruce Cork and his staff at the Argonne ZGS for their advice and help throughout this experiment.

References

[1]S. W. Kormanyos, A. D. Kirsch, J. R. O'Fallon, K. Ruddick, and L. G. Ratner, Phys. Rev. Letters 16, 709 (1966).

[2]R. J. Ott, J. Trischuk, J. Va'vra, T. J. Richards, and L. S. Schroeder, Phys. Letters 42B, 133 (1972).

[3]P. J. Duke, D. P. Jones, M. A. R. Kemp, P. G. Murphy, J. D. Prentice, and J. J. Thresher, Phys. Rev. 149, 1077 (1966).

[4]T. Dobrowolski, B. N. Gus'kov, M. F. Likhachev, A. L. Lubimov, Yu. A. Matulenko, V. S. Stavinsky, and A. S. Vovenko, Phys. Letters 24B, 203 (1967).

[5]A. S. Carroll, J. Fischer, A. Lundby, R. H. Phillips, C. L. Wang, F. Lobkowicz, A. C. Melissinos, Y. Nagashima, and S. Tewksbury, Phys. Rev. Letters 20, 607 (1968).

[6]W. F. Baker, P. J. Carlson, V. Chabaud, A. Lundby, J. Banaigs, J. Berger, C. Bonnel, J. Duflo, L. Goldzahl, and F. Plouin, Nucl. Phys. B9, 249 (1969).

[7]R. E. Rothschild, T. Bowen, P. K. Caldwell, D. Davidson, E. W. Jenkins, R. M. Kalbach, D. V. Petersen, and A. E. Pifer, Phys. Rev. D5, 499 (1972).

[8]E. S. Ma and G. L. Shaw, Phys. Rev. D3, 1264 (1971).

[9]T. A. Lasinski, A. Barbaro-Galtieri, R. L. Kelly, A. Rittenberg, A. H. Rosenfeld, T. G. Trippe, N. Barash-Schmidt, C. Bricman, V. Chaloupka, P. Söding, and M. Roos, Rev. Mod. Phys. 45, S1 (1973).

[11]There is some evidence of this resonance in the energy dependence of backward π^-p scattering. In the latter reaction isospin 1/2 resonances also contribute in the s channel. By adding the I = 1/2 resonances to the above I = 3/2 resonances we obtained a good fit to the π^-p data in reference 1. Likewise there is some evidence of structure at this energy derived from the π^+p total cross section data; when the $\Delta(2850)$ is subtracted from the isospin 3/2 total cross section, a bump remains at 3230 MeV/c^2 with a height of 0.5% of the total. See A. Citron, W. Galbraith, T. F. Kycia, B. A. Leontic, R. H. Phillips, A. Rousset, and P. H. Sharp, Phys. Rev. 144, 1101 (1966).

TABLE I

DIFFERENTIAL CROSS SECTIONS AT 180°
FOR π^+p BACKWARD ELASTIC SCATTERING

Po (GeV/c)	$\sqrt{S}$ (MeV)	$\frac{d\sigma}{d\Omega}\|_{180^\circ}$ (μb/sr)	$\frac{d\sigma}{du}\|_{180^\circ}$ (μb/GeV^2)
2.0	2160	$44.0\ ^{+10.1}_{-\ 8.2}$	$183\ ^{+42}_{-34}$
2.1	2200	$18.3\ ^{+\ 6.0}_{-\ 4.5}$	$74\ ^{+24}_{-18}$
2.2	2240	$71.5\ ^{+14.5}_{-12.1}$	$266\ ^{+54}_{-45}$
2.3	2290	$181.2\ ^{+15.6}_{-14.6}$	$638\ ^{+55}_{-51}$
2.4	2330	$291.9\ ^{+16.5}_{-15.5}$	$979\ ^{+55}_{-52}$
2.5	2370	$307.2\ ^{+14.7}_{-14.3}$	$982\ ^{+47}_{-46}$
2.6	2400	$312.6\ ^{+18.5}_{-17.4}$	$955\ ^{+57}_{-53}$
2.7	2440	$289.6\ ^{+13.1}_{-12.6}$	$847\ ^{+38}_{-37}$
2.8	2480	$255.5\ ^{+\ 6.6}_{-\ 6.5}$	$716\ ^{+19}_{-18}$
2.9	2500	$228.2\ ^{+10.1}_{-\ 9.2}$	$615\ ^{+27}_{-25}$
3.0	2560	$177.7\ ^{+\ 9.0}_{-\ 8.4}$	$460\ ^{+23}_{-22}$
3.1	2600	$135.2\ ^{+\ 8.6}_{-\ 8.1}$	$337\ ^{+21}_{-20}$
3.2	2630	$116.2\ ^{+\ 6.3}_{-\ 6.1}$	$280\ ^{+15}_{-15}$
3.3	2670	$89.3\ ^{+\ 5.6}_{-\ 5.3}$	$208\ ^{+13}_{-12}$

Po (GeV/c)	$\sqrt{S}$ (Mev)	$\frac{d\sigma}{d\Omega}\|_{180^\circ}$ (μb/sr)	$\frac{d\sigma}{du}\|_{180^\circ}$ (μb/GeV^2)
3.4	2700	$85.0^{+5.3}_{-5.0}$	191^{+12}_{-11}
3.5	2740	$83.8^{+5.3}_{-4.9}$	182^{+12}_{-11}
3.6	2770	$81.2^{+6.0}_{-5.5}$	171^{+13}_{-12}
3.7	2800	$74.9^{+4.7}_{-4.4}$	153^{+10}_{-9}
3.8	2830	$83.0^{+3.4}_{-3.3}$	165^{+7}_{-7}
3.9	2870	$83.3^{+3.7}_{-3.7}$	161^{+7}_{-7}
4.0	2900	$74.8^{+5.3}_{-4.8}$	140^{+10}_{-9}
4.1	2930	$75.4^{+4.1}_{-3.9}$	138^{+7}_{-7}
4.2	2960	$66.6^{+4.4}_{-4.2}$	118^{+8}_{-7}
4.3	3000	$62.3^{+5.0}_{-4.7}$	108^{+9}_{-8}
4.4	3030	$57.6^{+3.0}_{-3.0}$	$97.3^{+5.1}_{-5.1}$
4.5	3060	$48.8^{+5.0}_{-4.6}$	$80.4^{+8.2}_{-7.6}$
4.6	3090	$51.6^{+3.0}_{-3.0}$	$83.0^{+4.8}_{-4.8}$
4.7	3120	$50.7^{+4.6}_{-4.3}$	$79.6^{+7.2}_{-6.8}$
4.8	3150	$43.2^{+4.1}_{-3.9}$	$66.3^{+6.3}_{-6.0}$
4.9	3180	$50.4^{+5.0}_{-4.6}$	$75.7^{+7.5}_{-6.9}$
5.0	3210	$52.3^{+4.7}_{-4.3}$	$76.8^{+6.9}_{-6.3}$

Po (GeV/c)	$\sqrt{S}$ (MeV)	$\frac{d\sigma}{d\Omega}\Big\|_{180^\circ}$ (μb/sr)	$\frac{d\sigma}{du}\Big\|_{180^\circ}$ (μb/GeV^2)
5.1	3240	$47.9 \begin{smallmatrix}+4.1\\-3.7\end{smallmatrix}$	$68.8 \begin{smallmatrix}+5.9\\-5.3\end{smallmatrix}$
5.2	3270	$51.4 \begin{smallmatrix}+6.5\\-6.0\end{smallmatrix}$	$72.3 \begin{smallmatrix}+9.1\\-8.4\end{smallmatrix}$
5.3	3300	$50.7 \begin{smallmatrix}+5.1\\-4.9\end{smallmatrix}$	$69.9 \begin{smallmatrix}+7.0\\-6.8\end{smallmatrix}$
5.4	3320	$47.6 \begin{smallmatrix}+4.6\\-4.3\end{smallmatrix}$	$64.3 \begin{smallmatrix}+6.2\\-5.8\end{smallmatrix}$
5.6	3380	$38.7 \begin{smallmatrix}+4.7\\-4.1\end{smallmatrix}$	$50.3 \begin{smallmatrix}+6.1\\-5.3\end{smallmatrix}$
5.8	3430	$38.2 \begin{smallmatrix}+4.6\\-4.1\end{smallmatrix}$	$47.8 \begin{smallmatrix}+5.8\\-5.1\end{smallmatrix}$
6.0	3490	$30.9 \begin{smallmatrix}+4.3\\-3.7\end{smallmatrix}$	$37.3 \begin{smallmatrix}+5.2\\-4.5\end{smallmatrix}$

Figure Captions

Figure 1. Experimental layout.

Figure 2. The differential cross section for π^+p elastic scattering at 180^o. The solid curve is a fit to the data including the $\Delta(2200)$ and $\Delta(3230)$ resonances. The dashed portions show the effect of omitting these two resonances.

Figure 3. The energy dependence of the slope of the backward peak in π^+p elastic scattering.

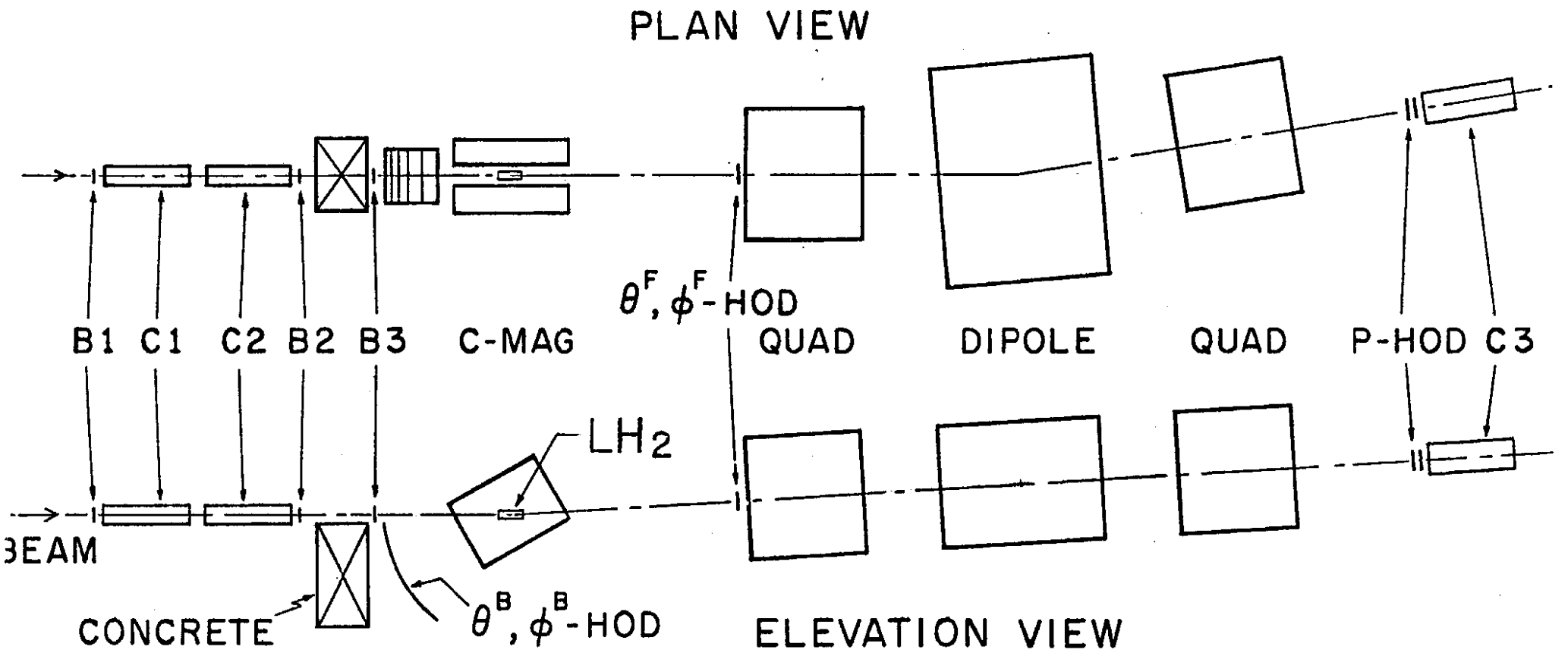
PLAN VIEW
B1
C1
C2
B2
B3
C-MAG
θ^F, ϕ^F-HOD
QUAD
DIPOLE
QUAD
P-HOD
C3
LH_2
BEAM
CONCRETE
θ^B, ϕ^B-HOD
ELEVATION VIEW

Fig. 1

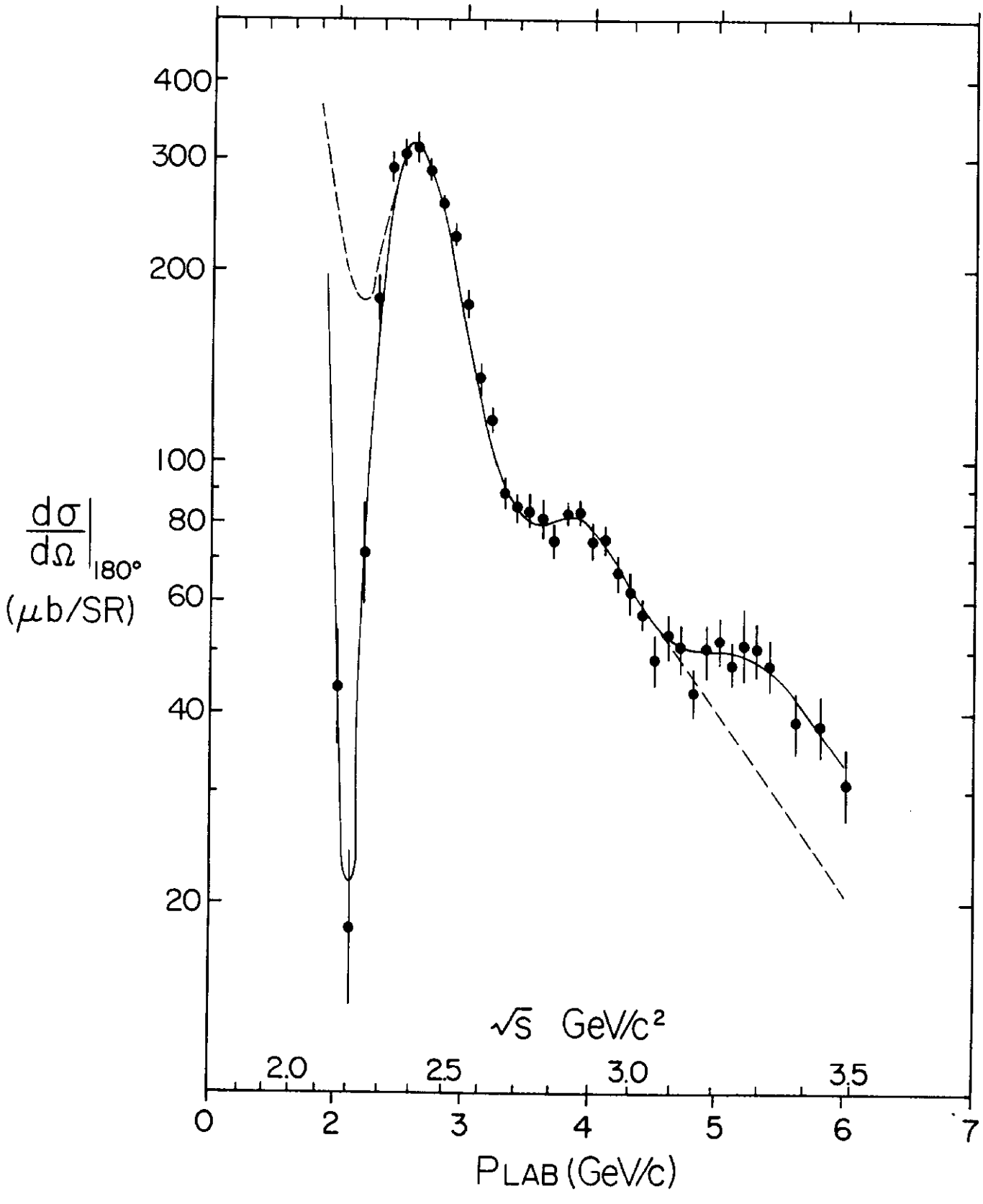
400
300
200
100
80
60
40
20
dσ/dΩ|180°
(μb/SR)
√s GeV/c²
2.0
2.5
3.0
3.5
0
2
3
4
5
6
7
PLAB (GeV/c)

Fig. 2

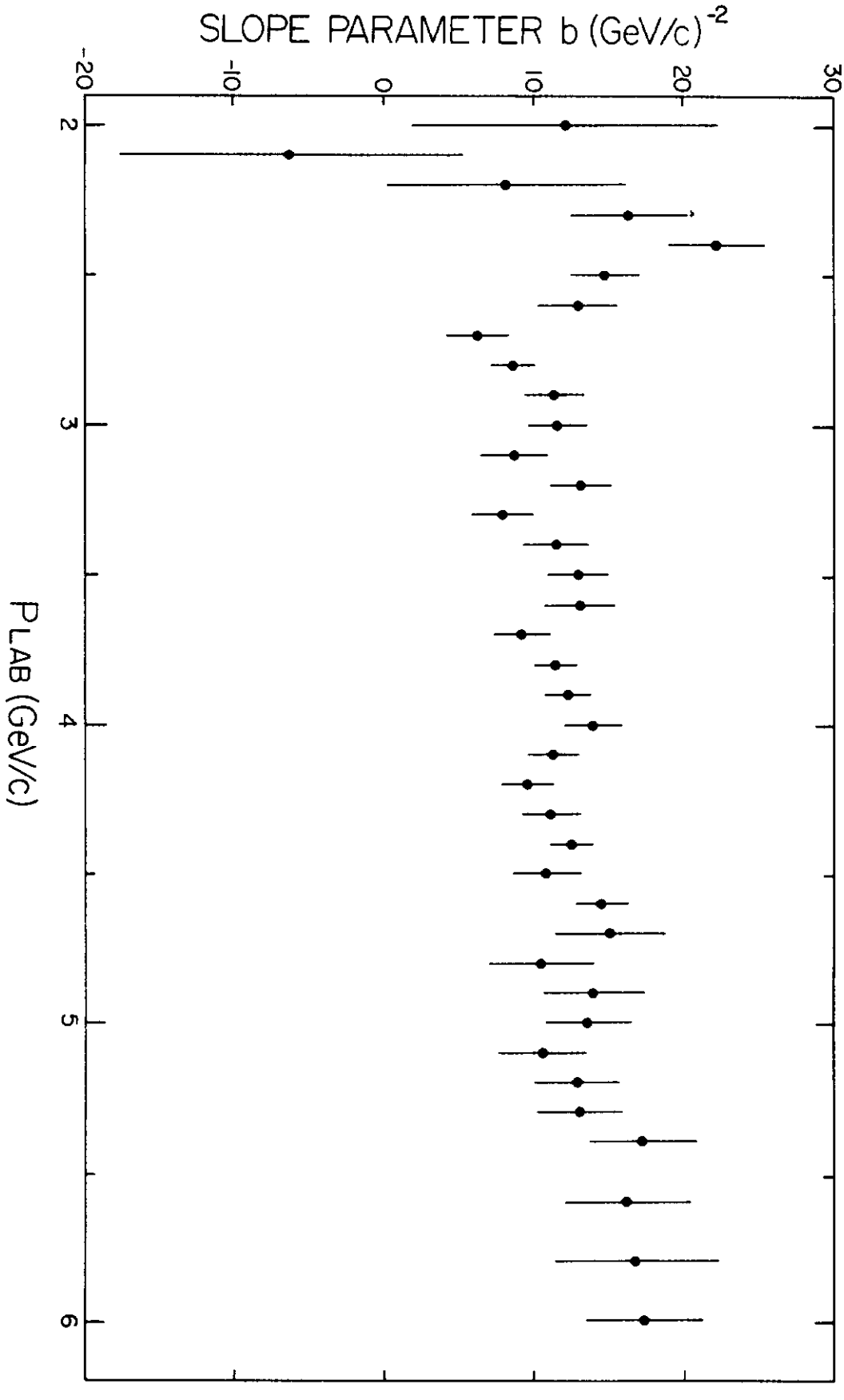

Fig. 3